J Inorg Organomet Polym (2017) 27:1482–1490
DOI 10.1007/s10904-017-0607-8

Synthesis of Poly(aniline/glycidyl methacrylate)-TiO_2 Nanocomposites via Gamma Irradiation and Their Electro-Responsive Characteristic

M. B. El-Arnaouty[1] · M. Eid[1] · M. Salah[1] · El-Sayed Soliman[2] · El-Sayed A. Hegazy[1]

Received: 22 April 2017 / Accepted: 19 June 2017 / Published online: 4 July 2017

Abstract Polyaniline/glycidyl methacrylate P(ANI/GMA) and Polyaniline/glycidyl methacrylate-TiO_2 [P(ANI/GMA)-TiO_2] nanocomposite materials have been prepared by gamma radiation. The synthesized polymers were characterized by X-ray diffraction pattern (XRD) which proving the existence of TiO_2 nanoparticles within the composite and the peaks related to the TiO_2 nanoparticles centered at $2\theta = 25.3°$, 27.5°, 37°, 38°, 41.37°, 48.1°, 54.26°, and 55.2°. The characteristic FTIR peaks of P(ANI) are shifted to a higher wave number in P(ANI/GMA)-TiO_2 nanocomposites due to interaction between TiO_2 and P(ANI/GMA). Morphological and structural properties of these composites have also been characterized by scanning electron microscopy (SEM). The thermal stability studies using thermogravimetric analysis (TGA) confirmed that the introduction of TiO_2 leads to increase the thermal stability. TEM image of P(ANI/GMA)-TiO_2 indicate that the particle size of TiO_2 was found to be with mean sizes 19 and 60 nm at TiO_2 content (0.1 and 0.5)%. The electrical conductivity measured using LCR Meter was around 10^{-3} S/cm which can be a good candidate as electro-conductive material.

Keywords Electroconductive material · P(ANI/GMA)-TiO_2 · SEM · X-ray · TEM

✉ M. Eid
mona_eid2000@yahoo.com

[1] Polymer Chemistry Department, National Center for Radiation Research and Technology, Atomic Energy Authority, Nasr City, P.O. Box 29, Cairo, Egypt

[2] Factually of Science, Ain Shams University, Cairo, Egypt

1 Introduction

The syntheses of polymer-inorganic hybrid nanoparticles with different combinations of the two components have attracted more and more attention, since they have interesting physical properties and potential applications [1]. In order to prepare the nanoscale materials successfully, several approaches have been employed, such as physical mixing, sol–gel techniques, in situ chemical polymerization in aqueous solution with the presence of monomer and inorganic particles, emulsion technology, so no-chemical processes and γ-irradiation techniques. Among these methods, the γ-irradiation technique is useful and has been extensively used to generate nanoscale metals and nanocomposites at room temperature under normal pressure. Moreover, this technique is easily controlled and adaptable, and it does not contribute impurities into the matrix [2].

Conducting polymers have recently aroused great interest among researchers because of their curious electronic, magnetic and optical properties. In terms of conducting polymers, polyaniline P(ANI) is one of the most studied electrically conducting polymers due to its good processibility, environmental stability and potential in the field of catalysis, biosensors, batteries, and electronic technology [3]. P(ANI) has a unique status due to the presence of reactive –NH–groups in the polymer chain flanked on either side by phenyl enerings, which imparts chemical flexibility to the system and improves the processibility to a large extent. Also, it is characterized by high chemical and thermal stability within the conductive form, low production costs and it can also be easily doped with inorganic and organic acids [4].

The aim of this work is preparation of P(ANI/GMA) and P(ANI/GMA)-TiO_2 nanocomposites by gamma radiation. The prepared samples were characterized by several

techniques including Fourier transform infrared spectroscopy (FTIR), X-ray diffraction (XRD), thermogravimetric analysis (TGA) and UV–Vis spectroscopy. Also their morphology was investigated by scanning electron microscopy (SEM), transmission electron microscopy (TEM) and electrical conductivity.

2 Materials and Techniques

2.1 Materials

Glycidyl methacrylate (2,3-epoxy propyl methacrylate) ≥97% (GC) and Titanium (IV) Oxide (TiO_2) <100 nm particle size, Sigma-Aldrich, Co. (USA). Aniline ($C_6H_5NH_2$) (for synthesis), Oxford laboratory, made in India. Hydrochloric acid and Methyl alcohol (99%) packed in Egypt by Beta Chem. for laboratory chemicals (Scheme 1).

2.2 Apparatus and Methods

2.2.1 Preparation of Polyaniline

Aniline (20%) was prepared by adding 20 ml of aniline (ANI) to 40 ml of HCl then dissolving in 40 ml of methanol. The mixture was stirred via magnetic stirrer for 2 h at room temperature. The solution was irradiated with 10 kGy using Co^{60} γ-ray that has activity 9100 curies at dose rate around 2 kGy/h. The irradiation chamber was constructed by the National Center for Radiation and Technology (NCRRT), Atomic Energy Authority of Egypt (AEAE) Cairo.

2.2.2 Preparation of P(ANI/GMA)

Radiation-induced polymerization method was used for the synthesis of P(ANI/GMA) as follows:

Firstly, Glycidyl methacrylate (GMA) was dissolved in methanol at the volume ratio (50:50) at room temperature. Then preparation of different compositions of polyaniline [P(ANI)]/Glycidyl methacrylate (GMA) [P(ANI/GMA)] at different volume ratios; (80:20), (70:30), (60:40), and (50:50) were prepared by adding the prepared polyaniline solution to Glycidyl methacrylate (GMA) solution then stirring via magnetic stirrer for 2 h. The mixture solutions were poured into test tubes then irradiated by gamma rays with different exposure doses (5, 10, 15, 20, 25, and 30) kGy.

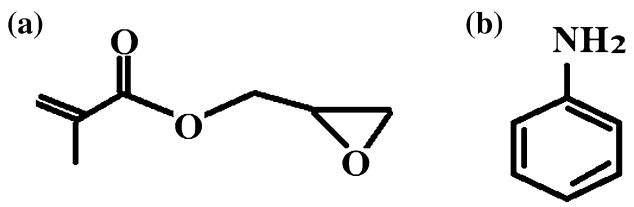

Scheme 1 Chemical structure: **a** Glycidyl methacrylate (2,3-epoxy-propyl methacrylate). **b** Aniline

2.2.3 Synthesis of P(ANi/GMA)-TiO_2 Nanocomposites

Preparation of polyaniline/Glycidyl methacrylate [P(ANI)/(GMA)] at the ratio (80:20) was carried out by adding the prepared polyaniline solution to GMA which dissolved in methanol at the volume ratio (50:50) then stirring via magnetic stirrer. Through the stirring process, different concentrations (0.1%, 0.5%) of nano-size titanium dioxide (TiO_2) were added to the mixture with continuous stirring for 2 h at room temperature then the mixture was sonicated for 12 min. The mixtures were poured into glass dishes then irradiated by gamma rays of 10 kGy. The obtained polymers were dried in oven at 70 °C for 24 h.

3 Characterization

3.1 FTIR Spectroscopy

FTIR of samples was performed according to ASTM E 1252-(02) "Standard Practice for General Techniques for Obtaining Infrared Spectra for Qualitative Analysis", using FTIR Perkin Elmer-Spectrum one in the range 400–4000 cm^{-1}.

3.2 Scan Electron Microscope (SEM)

JOEL JSM 5300 scanning electron microscope-Japan was used for investigating the morphology of different nanocomposites at high magnification and resolution by means of energetic electron beam.

3.3 X-ray Diffraction (XRD)

XRD of samples was performed according to XRD spectrophotometer, Model (X'pert Pro), Manufacture (PAN analytical) equipped with X-ray tube [Cu target, 40 KV (Voltage), 30 (mA) (current)], the X-ray data were recorded in a range from 4 to 80 (degree) 2θ with continuous scanning mode and scanning speed 8 (deg/min). The average particle size of the nanoparticles was calculated from the full width at half maximum (FWHM) and the peak position of XRD line broadened according to the Scherrer equation.

$$d = K\lambda/\beta\cos\theta \quad (1)$$

where d is the particle size, K = 0.89 is the Scherrer constant related to the shape and index (hkl) of the crystals, λ is the wavelength of the X-ray (Cu Ka, 1.54056 Å), θ is the diffraction angle, and β is the full width at half maximum (FWHM in radian) [5].

3.4 Thermogravimetric Analysis (TGA)

Thermogravimetric analysis was performed according to TGA-DSC, Model SDTQ 600 (USA), the temperature ranged from ambient temperature to 600 °C at a heating rate of 10 °C/min. The primary TGA thermograms were used to determine the thermal stability and rate of thermal decomposition of different nanocomposites.

3.5 High Resolution Transmission Electron Microscopy (HRTEM)

High resolution transmission electron microscopy (HRTEM) measurements were performed with a (JEOL, JEM 2100, Japan) operating at 200 kV. High resolution transmission electron microscopy (HRTEM) was used to find out the size of different nanocomposites. To image the nanocomposites on HRTEM, finely grounded nanocomposites samples were dispersed in 1 ml of ethanol followed by sonication to get a solution of composite nanoparticles. Approximately 10–20 µL of this solution was dropped on a 3 mm copper grid, drying at room temperature. The copper grid was inserted into transmission electron microscope.

3.6 Electrical Conductivity Measurements

Electrical conductivity measurements were performed by using LCR Meter (TEGAM), Model 3550.

4 Results and Discussion

4.1 FT-IR Measurements

The analysis of the structural information concerning P(ANI/GMA), and P(ANI/GMA)-TiO_2 nanocomposites samples have been investigated by FTIR spectroscopy. The characteristic bands of P(ANI/GMA) and P(ANI/GMA)-TiO_2 nanocomposites are shown in Fig. 1. From Fig. 1a, the FTIR spectra of P(ANI/GMA) particles indicate the C=C stretching vibration bands which attributed to the quinonoid and benzenoid units appeared at 1602 and 1496 cm^{-1}, respectively. Stretch vibration of the N–H bonds was appeared at 3353 cm^{-1} [6]. The peaks around 2964 and 2875 cm^{-1} represent the (C–H) asymmetric and symmetric in CH_3 and CH_2 group, where the peaks at 1480 and 1350 cm^{-1} represent the bending vibration for CH_2 and

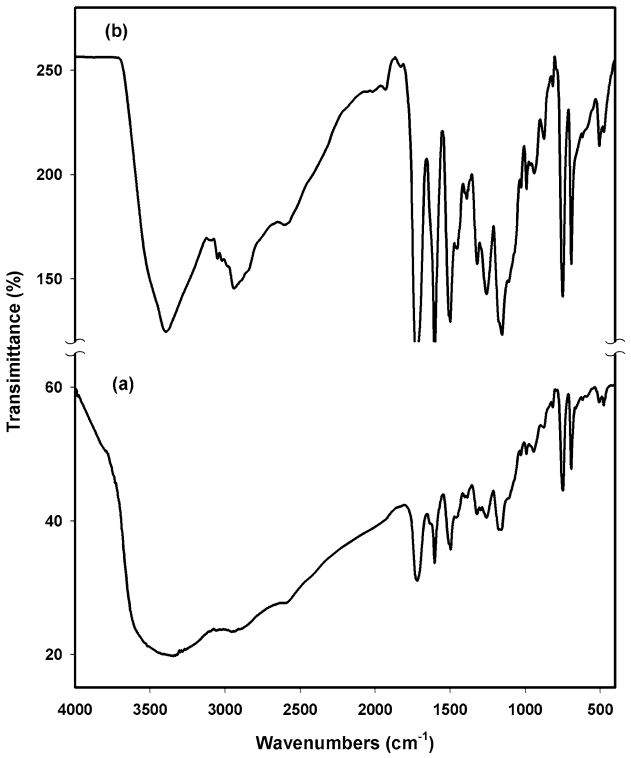

Fig. 1 FTIR spectra of (*a*) P(ANI/GMA) and (*b*) P(ANI/GMA)-TiO_2 (0.5%) at irradiation dose 10 kGy

CH_3 Groups [7]. In addition, a stretching band at 1320 cm^{-1} assigned to C–N was also observed [8, 9]. On the other hand, the special absorption band at 1719 and 1161 cm^{-1} were corresponded to the carbonyl C=O group originated from the P(GMA) core and C–O stretching vibration. Three bands of C–O–C stretching, a medium intensity symmetric stretching vibration at about 1257 cm^{-1}, a medium intensity asymmetric band at 943 cm^{-1}, and a strong band at 748 cm^{-1} may be attributed to the epoxide ring. The spectrum also showed a strong band at 692 cm^{-1} which attributed to (=C–H) of aromatic ring [10].

In Fig. 1b, the P(ANI/GMA)-TiO_2 nanocomposites spectrum shows the same characteristic peaks, in addition to the peak at 670 cm^{-1} which corresponding to Ti–O stretching [11]. On adding TiO_2 nanoparticles to P(ANI/GMA), there is a displacement of 3353 to 3391 cm^{-1} and 1719 to 1724 cm^{-1}. It is obvious that the corresponding peaks were shifted to the higher wave number and their intensities were changed after the addition of TiO_2 nanoparticles. In addition, the methylene vibration band shifts from 2964 to 2940 cm^{-1}. These significant changes suggest that an interfacial interaction exists between the P(ANI) and its inorganic counterpart of TiO_2 nanoparticles, where the titanium in titania has an intense tendency to form coordination complexes with the nitrogen atoms in P(ANI) macromolecules. Similar observation has been reported by Lee et al.

[12]. From the figure it can be showed that, the absorption intensity is increased by adding TiO_2 nanoparticles in the case of nanocomposites due to uniform distribution of TiO_2 nanoparticles in nanocomposites matrix and elimination of agglomeration [13].

4.2 SEM Measurements

Scanning electron microscopy is the most widely employed technique used for investigation the shape, morphology, and porosity of the polymer matrices. Figure 2a shows SEM image of P(ANI/GMA). The image showed that the surface was rough, coated with irregular granule shape particulates with uneven lumps and holes, indicating the successful coating of P(ANI). The SEM image of P(ANI/GMA) exhibits an amorphous surface looks like spongy shaped [14].

Figure 2b, c shows the SEM images of P(ANI/GMA)-TiO_2 at different TiO_2 contents, it can be seen that, all the nanocomposites reveal granular shaped structure, in which the size of pores reduces as TiO_2 nanoparticles content increases [15]. It is found that the doping of TiO_2 strongly affected the morphology of the resulting P(ANI/GMA)-TiO_2 nanocomposites. In case of P(ANI/GMA)-TiO_2 nanocomposite, the SEM micrograph revealed a granular structure looks like coral reefs with an interlocking arrangement. This suggests that the most of TiO_2 nanoparticles were coated with PANI [16]. The distribution and packing of TiO_2 in the P(ANI/GMA) matrix is more uniform, and no large lumps are observed [17].

The SEM images show the doping of TiO_2 nanoparticles has a strong effect on the morphology of P(ANI/GMA), since P(ANI) has various structures such as granules, nanofibers, nanotubes, nano-spheres, microspheres and flakes [9].

4.3 X-ray Diffraction Measurements (XRD)

XRD was used to examine the structure of synthesized P(ANI/GMA) and P(ANI/GMA)-TiO_2 nanocomposite and to investigate the effect of TiO_2 nanoparticles on the P(ANI/GMA) structure. Figure 3a, b shows the XRD pattern of P(ANI/GMA) and P(ANI/GMA)-TiO_2 at TiO_2 concentration 0.5%. From Fig. 3a, it can be seen that, XRD pattern of P(ANI/GMA) reveals more than one crystalline peak appeared at $2\theta = 21°$, 22°, 26.7°, and 35.6° with one broad amorphous peak centered at $2\theta = 16°$. The peaks observed at 21°, 22°, 26.7°, and 35.6° can be ascribed to periodicity parallel and perpendicular to P(ANI) conjugation chains, respectively [18]. The crystalline peak is indicating that HCl doped P(ANI) is not fully amorphous as well as π–π interchain stacking has improved [19, 20]. According to Fig. 3b, the XRD patterns of P(ANI/GMA)-TiO_2

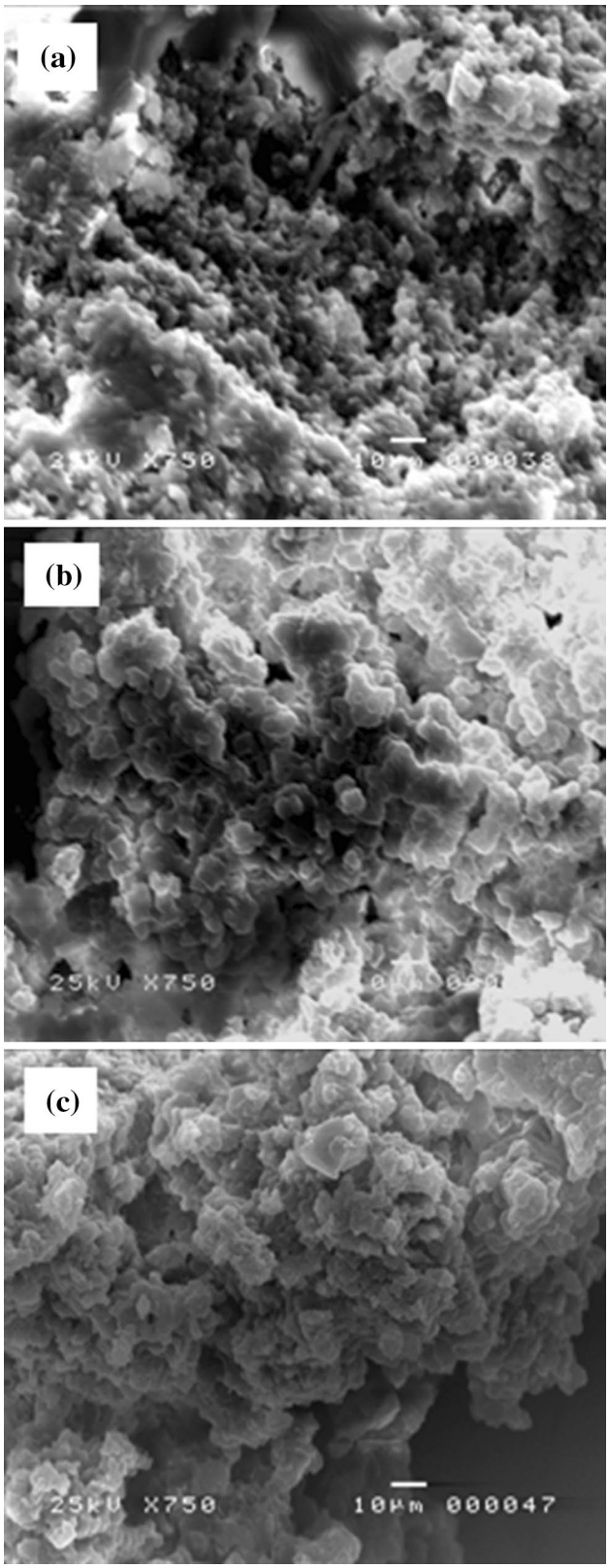

Fig. 2 SEM micrographs of (**a**) P(ANI/GMA), **b** P(ANI/GMA)-TiO_2 (0.1%) and **c** P(ANI/GMA)-TiO_2 (0.5%) at irradiation dose 10 kGy

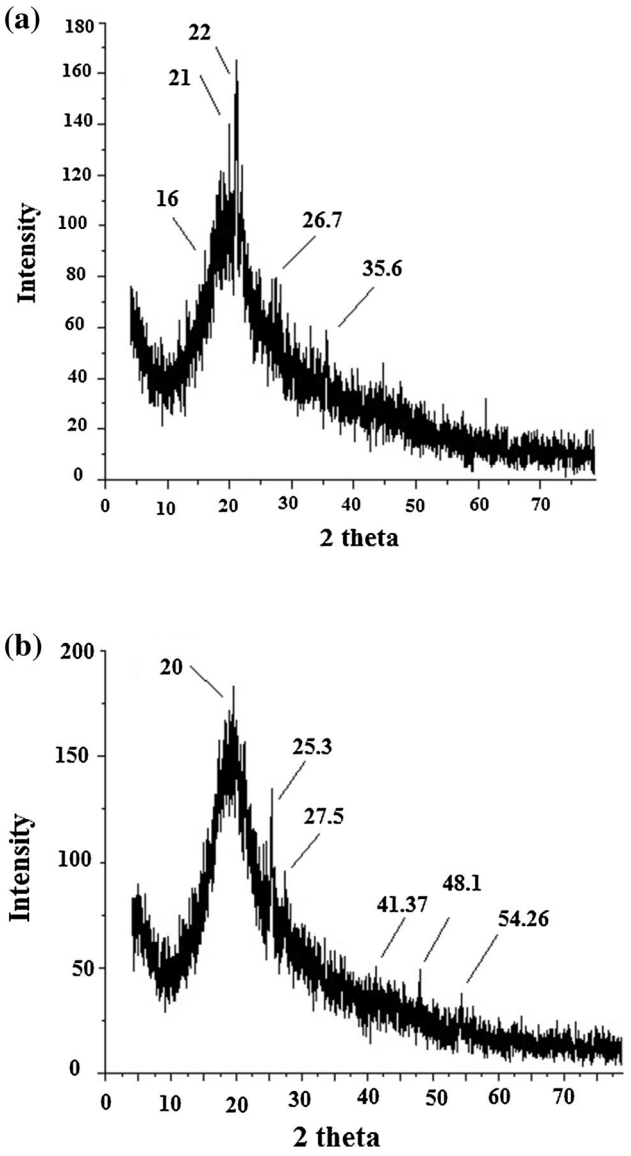

Fig. 3 X-ray diffraction of (**a**) P(ANI/GMA) and (**b**) P(ANI/GMA)-TiO_2 (0.5%) at irradiation dose 10 kGy

Table 1 Summary of the average particle size of TiO_2 (0.5%) nanoparticles

Angle (2θ)	θ	Cos θ	FWHM	d [Particle size (nm)]
25.33	12.665	0.9757	0.1181	65.1
27.53	13.765	0.97127	0.2362	32.7
37	18.5	0.94832	0.0900	87.9
38	19	0.94551	0.0900	88.2
48.12	24.06	0.91311	0.5510	14.9
54.26	27.13	0.88997	0.4723	17.8
55.21	27.605	0.88616	0.0900	94.1

nanocomposites shows the characteristic peaks not only for the P(ANI/GMA) but also for the TiO_2 nanoparticles, proving the existence of TiO_2 nanoparticles within the composite. In case of P(ANI/GMA)-TiO_2 nanocomposite samples of TiO_2 concentrations at 0.5%, an amorphous peak have been appeared at $2\theta = 20°$, whereas the peaks related to the TiO_2 nanoparticles centered at $2\theta = 25.3°$, 27.5°, 41.37°, 48.1°, and 54.26°. These results mean that, there is an interaction of TiO_2 nanoparticles and P(ANI/GMA) by formation of hydrogen bonding between H–N and oxygen of TiO_2 [20].

The P(ANI/GMA)-TiO_2 have more intensive lines and smooth peaks, which indicate clearly that the degree of ordering increase and the crystallinity content increase according to Scherrer equation [5, 21]. The shape factor is used in X-ray diffraction and crystallography to correlate the size of sub-micrometre particles, or crystallites, in a solid to the broadening of a peak in a diffraction pattern.

The average grain size of TiO_2 nanoparticles was calculated using Scherrer equation from the half maximum width and the peak position of XRD line broadened. According to Scherrer equation, the average particle size of TiO_2 nanoparticles in the P(ANI/GMA)-TiO_2 (0.5%) nanocomposites are represented in Table 1.

From the data, it can be noticed that the average particle size of P(ANI/GMA)-TiO_2 (0.5%) found to be 57.2 nm. This result indicate that there is no chance of aggregations to form large particle size at TiO_2 content (0.5%) [22].

4.4 Thermogravimetric Analysis (TGA)

Thermogravimetric analysis considered the most practical widely used method to illustrate the thermal stability of polymers over a wide range of temperature. Moreover, to give a better understanding of the thermal stability of polymers, the rate of thermal decomposition (dw/dt) was plotted as a function of decomposition temperature.

Figure 4a–c, represents the TGA curve of P(ANI/GMA), P(ANI/GMA)-TiO_2 (0.1% and 0.5%) at irradiation dose of 10 kGy. Figure 4a represents the multistage thermal degradation of the P(ANI/GMA). The first stage is up to 172 °C due to the evolution of moisture with thermal decomposition percent 5.3%. The second stage, up to 303 °C, may be due to decomposition of the function groups in the side chain of the polymer with thermal decomposition percent 27.4%. The major decomposition temperatures were within 346 to 413 °C and 600 °C with thermal decomposition percent of 47.6, 76.8, and 93.2%, respectively which may be due to the anhydride formation and backbone degradation, respectively [21, 23].

The TGA and the rate of thermal decomposition (dw/dt) curve for P(ANI/GMA)-TiO_2 (0.1%) nanocomposite are shown in Fig. 4b. It can be noted that, there are

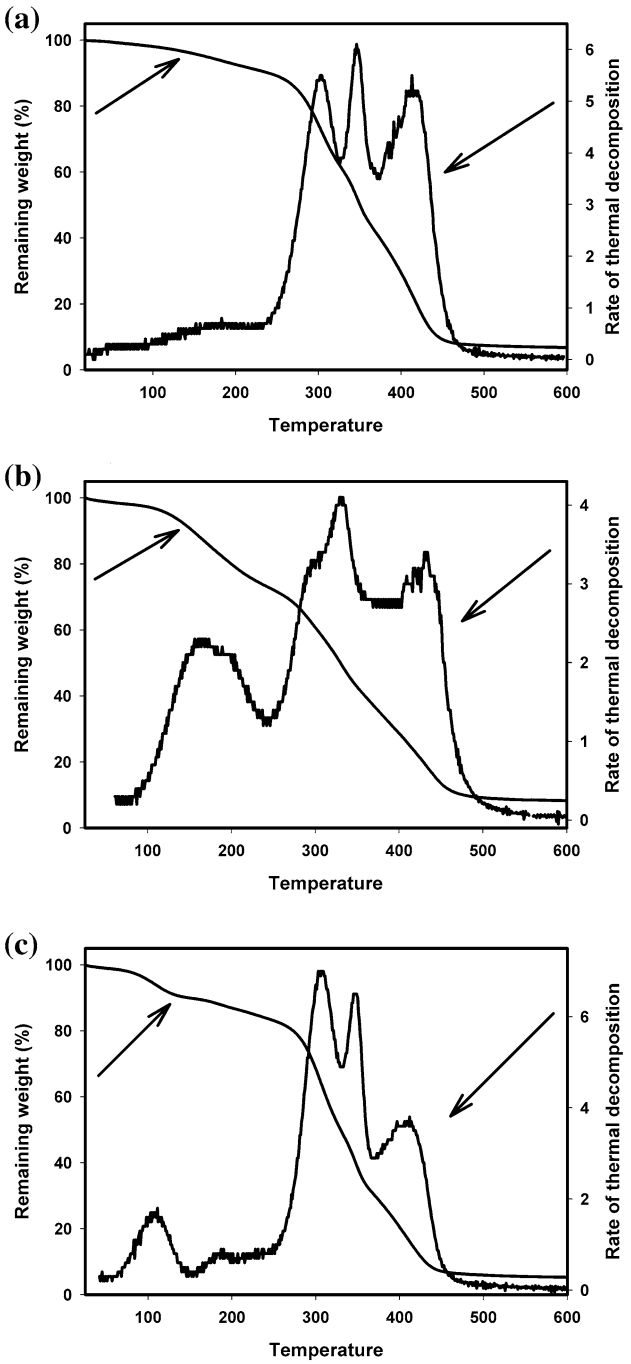

Fig. 4 The TGA curve of (**a**) P(ANI/GMA), **b** P(ANI/GMA)-TiO_2 (0.1%) and **c** P(ANI/GMA)-TiO_2 (0.5%) at irradiation dose of 10 kGy

multi-decomposition stages. The first stage up to 169 °C may be due to evaporation of some residual water present in the matrix with degraded weight percent of 13.8%. The second stage, up to 308 °C, may be due to decomposition of the function groups in the side chain of the polymeric materials and desorption of TiO_2 nanoparticles which presents in the side chains with degraded weight percent 39.9%. The major decomposition temperatures were found with range from 329 °C to 429 °C with degraded weight percent 48.4 and 77.3% respectively, which can be attributed to main chain breakdown. The final decomposition temperature at 600 °C may suggested the carbonization prevails with degraded weight percent of 91.7% [14].

The thermal degradation of the P(ANI/GMA)-TiO_2 (0.5%) represents in Fig. 4c shows a multi-degradation stages. The evaporation of some residual water present in the matrix occurs in the first stage at 107 °C with degraded weight percent of 5.2%. The second stage and third stage at 190 and 308 °C may be due to decomposition of the function groups in the side chain of the polymer and desorption of TiO_2 nanoparticles presents in the side chains with degraded weight percent 12.1 and 34.3% respectively. The main decomposition temperatures were at 347 and 412 °C with degraded weight percent 57.7 and 79.9% respectively. Increasing the degradation temperature up to 600 °C shows degraded weight percent of 93% which may be due to the carbonization prevails [14, 24].

It is clear from Table 2 that the temperature at which the maximum temperature value of the rate decomposition (T_m) increased by incorporation of TiO_2 (0.1 and 0.5%) into P(ANI/GMA). From Fig. 4 and Table 2, according to the remaining weight percent in the final stage at 600 °C, it can be concluded that the incorporation of TiO_2 increase the remaining weight percent for different TiO_2 contents and also decreases the maximum rate of thermal decomposition and increase for most of samples which indicating the increase of thermal stability [9].

4.5 High Resolution Transmission Electron Microscopy (HRTEM)

To determine the size and shape of the majority of TiO_2 nanocomposites, the polymeric nanocomposites were crushed according to the procedure mentioned in the experimental section and the supernatants were viewed under HRTEM which present in Fig. 5a–c. As seen in Fig. 5a, P(ANI/GMA) showed a disordered amorphous structure. It can be observed that, a rough P(ANI) shell formed around the P(GMA) surface and the particle size in the range was found to be between 13 and 24 nm. Figure 5b, c shows HRTEM images of P(ANI/GMA)-TiO_2 nanocomposites at TiO_2 concentrations 0.1 and 0.5% respectively. By increasing TiO_2 content the possibility of agglomeration increases which resulting the increase of TiO_2 particle size [9].

Figure 6a–c represent the particle size distribution percent of P(ANI/GMA) and P(ANI/GMA)-TiO_2 at different TiO_2 content percent 0.1 and 0.5% respectively. The results indicate that the TiO_2 particle size in P(ANI/GMA)-TiO_2 at content 0.1 and 0.5% was range between (8–77) and (39–95) nm respectively, with mean sizes 19 and 60 nm

Table 2 Rate of thermal decomposition of P(ANI/GMA)-TiO_2 nanocomposites with different TiO_2 contents and temperatures of maximum values of the rate of their decomposition (T_m)

Sample description	Temperature (°C)	Remaining weight (%)	Rate of thermal decomposition (dw/dt)	Tm (°C)	Remaining weight (%) at 600 °C
P(ANI/GMA)	172	94.7	0.6	172	6.8
	303	72.6	5.56	303	
	346	52.4	6.05	346	
	413	23.2	5.52	413	
P(ANI/GMA)-TiO_2 (0.1%)	169	86.2	2.3	169	8.3
	308	60.1	3.44	308	
	329	51.6	4.06	329	
	429	22.7	3.4	429	
P(ANI/GMA)-TiO_2 (0.5%)	107	94.8	1.8	107	7
	190	87.9	0.8	189.5	
	308	65.7	6.9	307.9	
	347	42.3	6.4	346.5	
	412	20.1	3.6	411.6	

for P(ANI/GMA)-TiO_2 at TiO_2 concentrations 0.1 and 0.5% respectively. The results of HRTEM were found to be in good agreement with the results that calculated using Scherrer equation from the half maximum width and the peak position of XRD line broadened.

4.6 Electrical Conductivity Measurements

Electrical conductivities of P(ANI/GMA) and P(ANI/GMA)-TiO_2 nanocomposites at TiO_2 content percent 0.5% are illustrated in Table 3. The range of electrical conductivity of P(ANI) is wide spread from 10^{-10} to 10^{-3} S/cm based on the acid doping and fillers [25]. Electrical conductivity of P(ANI/GMA)-TiO_2 nanocomposites results show that electrical conductivity of P(ANI/GMA) decreased on adding TiO_2 from 1.343×10^{-3} to 0.765×10^{-3}. This results can be attributed to interaction between –NH of P(ANI) with TiO_2 nanoparticles and bond formation in the structure. In addition, the decrease of conductivity of P(ANI/GMA)-TiO_2 nanocomposites may be ascribed to the behavior of TiO_2 in the nanocomposites or reduction of the doping degree [26]. According to Mostafaei and Zolriasatein [27] the conductivity of the polymer depends on the nature of dopant and the inorganic materials concentration, which have an important role in conductivity of the nanocomposites [9].

5 Conclusion

The synthesis of P(ANI/GMA) and P(ANI/GMA) TiO_2 nanocomposites has been demonstrated using gamma radiation. FTIR results revealed that a chemical interaction between P(ANI/GMA) and TiO_2 was established. Scan electron microscope (SEM) showed that TiO_2 nanoparticles had a significant effect on the morphology, since the TiO_2 nanoparticles are packing in the P(ANI/GMA) matrices with uniform distribution. It can also showed that, the pore size reduces as TiO_2 nanoparticles content increase. XRD investigation indicates that, the P(ANI/GMA) has crystalline peaks appeared at $2\theta = 21°$, 22°, 26.7°, and 35.6° beside the amorphous one centered at $2\theta = 16°$. Addition of TiO_2 to P(ANI/GMA) composite show the TiO_2 related peaks and the intensities of the peaks increase by increasing the TiO_2 content. The particle size calculated by Scherrer equation indicates the nanosize of TiO_2 and the particle size increase by increasing the TiO_2 content.

The thermal stability study of different products indicates the increase in the thermal stability by adding the TiO_2 and also by increasing the TiO_2 content. A new thermal degradation stage has appeared in the region (142–251) °C by increasing the TiO_2 contents in P(ANI/GMA) and also increase of the remaining weight percent which indicating the increase of thermal stability. Transmission electron microscope investigate the size and shape of the majority of TiO_2 nanoparticles. The results indicate that, a rough P(ANI) shell formed around the P(GMA) surface. By increasing the TiO_2 content, the possibility of agglomeration formation increases which resulting in the increase of TiO_2 particle size. The results of TEM are nearly acceptable with the average particle size of TiO_2 nanoparticles that calculated using Scherrer equation. Electrical conductivity results of P(ANI/GMA)-TiO_2 indicated that, the conductivity of the composites was decreased due to the interfacial interaction between the polymer and TiO_2 counterparts.

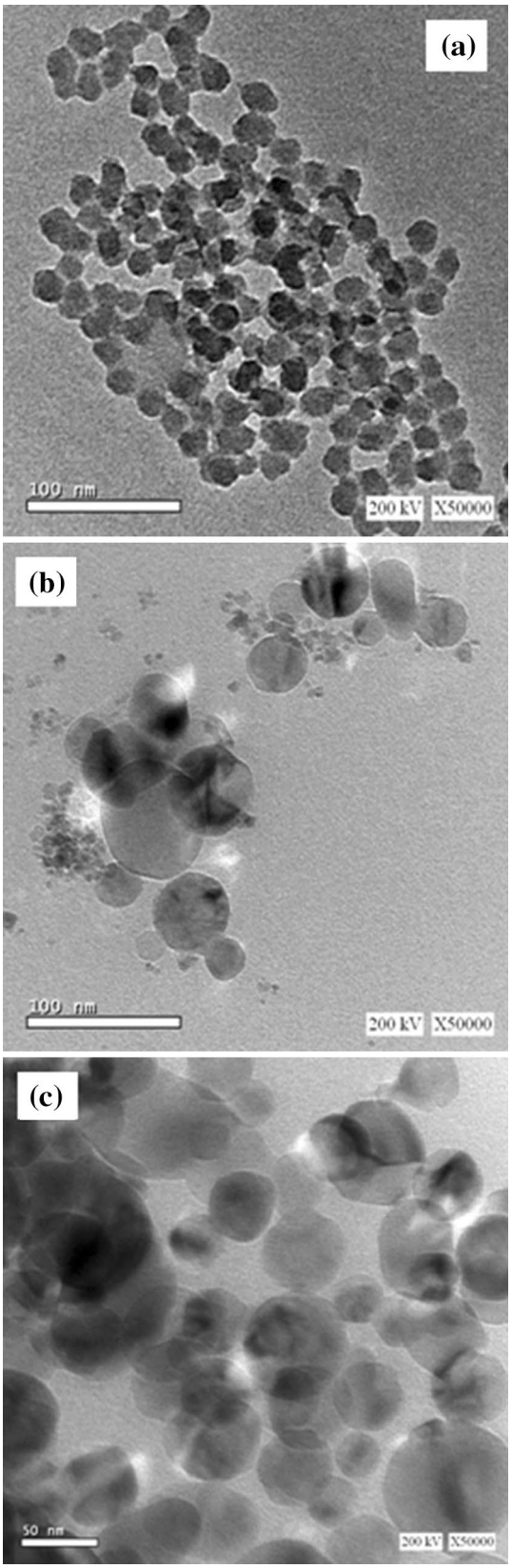

Fig. 5 TEM images of (**a**) P(ANI/GMA) and P(ANI/GMA)-TiO_2 nanocomposites at different TiO_2 content percent (**b**) 0.1% and (**c**) 0.5% at irradiation dose 10 kGy

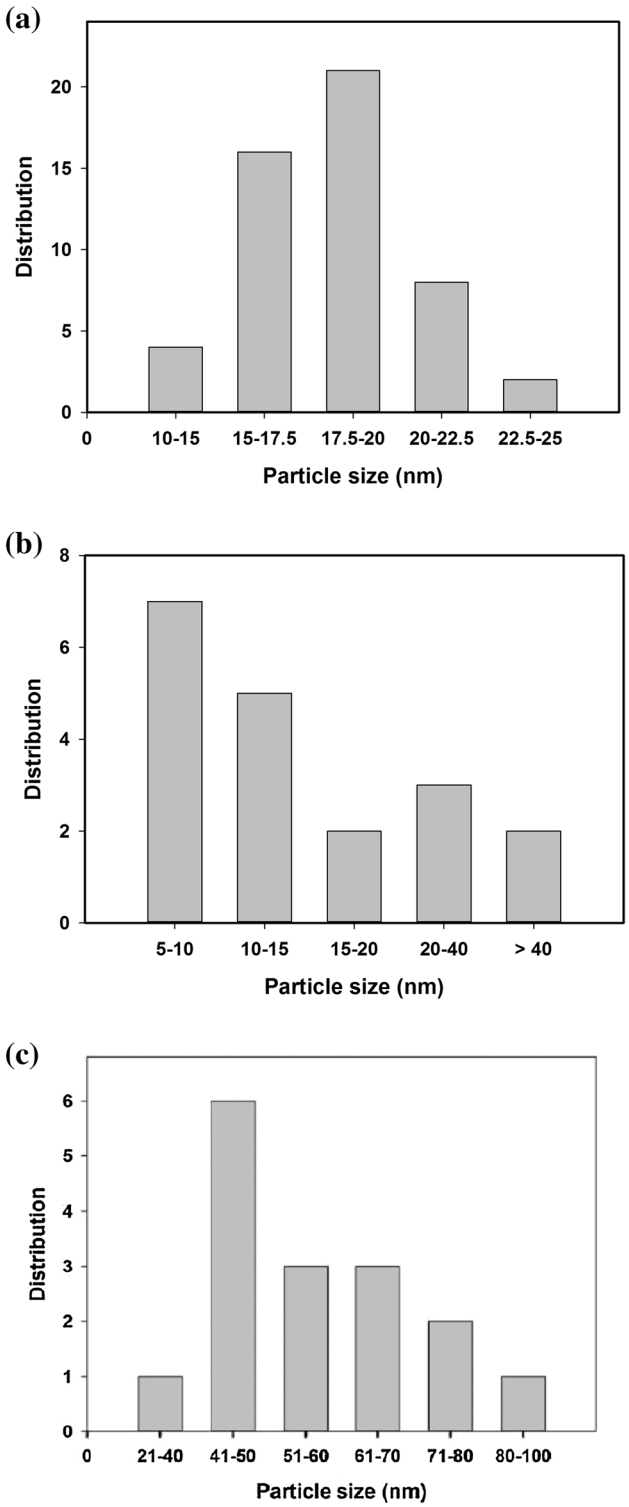

Fig. 6 Corresponding size distribution histogram of (**a**) P(ANI/GMA) and P(ANI/GMA)-TiO_2 nanocomposites at TiO_2 content percent (**b**) 0.1%, (**c**) 0.5% at irradiation dose 10 kGy

Table 3 The electrical conductivity of P(ANI/GMA) and P(ANI/GMA)-TiO_2 nanocomposites with TiO_2 content 0.5% at irradiation dose 10 kGy

Copolymeric composition	Electrical conductivity (S/cm)
P(ANI/GMA)	1.343×10^{-3}
P(ANI/GMA)-TiO_2 (0.5%)	0.765×10^{-3}

References

1. M.R. Karim, K.T. Lim, C.J. Lee, M.T.I. Bhuiyan, H.J. Kim, L.-S. Park, M.S. Lee, J. Polym. Sci. Part A **45**, 5741 (2007)
2. F.X. Liu, M. Tang, L. Liu, S. Lu, J.Y. Wang, Z.Y. Chen, R. Ji, Enhanced Phys. Status Solidi **179**, 437 (2000)
3. M.R. Karim, C.J. Lee, Y.-T. Park, M.S. Lee, Synth. Met. **151**, 131 (2005)
4. K.H. Hong, T.J. Kang, J. Appl. Polym. Sci. **99**, 1277 (2006)
5. A. Patterson, Phys. Rev. **56**, 978 (1939)
6. X.W. Li, W. Chen, C.Q. Bian, J.B. He, N. Xu, G. Xue, Appl. Surf. Sci. **217**, 16 (2003)
7. M. Varga, J. Prokes, P. Bober, J. Stejskal, WDS'12 Proceedings of Contributed Papers, Part III, **52** (2012)
8. M.B. El-Arnaouty, A.M. Abdel Ghaffar, M.E. Aboulfotouh, N.H. Taher, A.A. Taha, Polym. Bull. **72**, 2739 (2015)
9. A. Mostafaei, F. Nasirpouri, Prog. Org. Coat. **77**, 146 (2014)
10. M. Herring, J. Macromol. Sci. Polym. Rev. **46**(3), 245 (2006)
11. K. Gurunathan, D.P. Amalnerker, D.C. Trivedi, Mater. Lett. **57**, 1642 (2003)
12. I.S. Lee, J.Y. Lee, J.H. Sung, H.J. Choi, Synth. Met. **152**, 173 (2005)
13. M.R. Karim, J.H. Yeum, M.S. Lee, K.T. Lim, React. Funct. Polym. **68**, 1371 (2008)
14. W.L. Zhang, S.H. Piao, H.J. Choi, J. Colloid Interface Sci. **402**, 100 (2013)
15. M. Eid, M.B. El-Arnaouty, M. Salah, E.S. Soliman, E.A. Hegazy, J. Polym. Res. **19**, 9835 (2012)
16. S. Sathiyanarayanan, S. Syed Azim, G. Venkatachari, Electrochim. Acta **52**, 2068 (2007)
17. K.E. Strawhecker, E. Manias, Chem. Mater. **12**, 2943 (2000)
18. C. Barthet, S.P. Armes, S.F. Lascelles, S.Y. Luk, H.M.E. Stanley, Langmuir **14**, 2032 (1998)
19. L. Kwanghee, C. Shinuk, H.P. Sung, A.J. Heeger, L. Chan-Woo, L. Suck-Hyun, Nat. Lett. **441**, 65 (2006)
20. L. Shi, X. Wang, L. Lu, X. Yang, X. Wu, Synth. Met. **159**, 2525 (2009)
21. M. Eid, D.E. Hegazy, J. Inorg. Organomet. Polym. Mater. **22**, 985 (2012)
22. M.B. El-Arnaouty, M. Eid, Polym. Plast. Technol. Eng. **49**, 182 (2010)
23. F. Li, X. Xu, Q. Li, Y. Li, H. Zhang, J. Yu, A. Cao, Polym. Degrad. Stab. **91**, 1685 (2006)
24. E.A. Hegazy, H.A. Abd El-Rehim, N.A. Khalifa, S.M. Atwa, H.A. Shawky, Polym. Int. **43**, 321 (1997)
25. Y. Long, Z. Chen, N. Wang, J. Li, M. Wan, Physica B **344**, 82 (2004)
26. J. Deng, C.L. He, Y. Peng, J. Wang, X. Long, P. Li, A.S.C. Chan, Synth. Met. **139**, 295 (2003)
27. A. Mostafaei, A. Zolriasatein, Prog. Natl. Sci.: Mater. Inter. **22**, 273 (2012)